NUCLEAR SCIENCE AND ENGINEERING: **121**, 468–482 (1995)

Modeling Water Chemistry, Electrochemical Corrosion Potential, and Crack Growth Rate in the Boiling Water Reactor Heat Transport Circuits—I: The DAMAGE-PREDICTOR Algorithm

Tsung-Kuang Yeh, Digby D. Macdonald, and Arthur T. Motta

The Pennsylvania State University, 517 Deike Building, University Park, Pennsylvania 16802

Received November 9, 1994
Accepted March 28, 1995

Abstract—*A computer code with the capability of simultaneously estimating the concentrations of radiolysis species, the electrochemical corrosion potential, and the kinetics of growth of a reference crack in sensitized Type 304 stainless steel is developed for the heat transport circuits of boiling water reactors (BWRs). The primary objective of this code, DAMAGE-PREDICTOR, is to theoretically evaluate the effectiveness of hydrogen water chemistry (HWC) in the BWRs as a function of feedwater hydrogen concentration and reactor power level. The power level determines various important thermal-hydraulic parameters and the neutron and gamma energy deposition rate in the core and near-core regions. These input parameters are estimated using well-established algorithms, and the simulations are carried out for full-power conditions for two reactors that differ markedly in their responses to HWC. The DAMAGE-PREDICTOR code is found to successfully account for plant data from both reactors using a single set of model parameter values.*

I. INTRODUCTION

As the operating boiling water reactors (BWRs) in the United States age, the frequency of incidents of intergranular stress corrosion cracking (IGSCC) and irradiation-assisted stress corrosion cracking (IASCC) of stainless steel components in the primary heat transport circuits (HTCs) is increasing. In particular, concern has arisen over the cracking of BWR in-vessel components, such as the core-shroud, upper plenum structure, and jet pumps. The most important issue would be the cracking of components in the lower plenum, which contains the control rod drives, because of the safety implications and because of the considerable cost of repair.

The most promising solution to this problem may be hydrogen water chemistry (HWC). In this technique, hydrogen (H_2) is added to the reactor feedwater to reduce the oxygen and hydrogen peroxide concentrations and ultimately the electrochemical corrosion potential (ECP). However, this technique is not without problems because the generation of mildly reducing conditions within the HTC results in the transfer to the steam phase of nitrogen and/or ammonia, containing radioactive ^{16}N. Under oxidizing conditions, this could lead to oxyanions of nitrogen remaining in the water (and hence in the primary circuit). The volatile ammonia is transported to the condensers, and the resulting radiation fields exact a high man-rem cost on the utilities, which must be balanced against the potential benefits of HWC. Furthermore, it is not at all clear that HWC is effective in protecting some components against IGSCC and IASCC, particularly those in-vessel components that are exposed to high gamma and neutron fields. Importantly, the level of effectiveness appears to depend strongly on the particular reactor under consideration. Thus, Ruiz et al.,[1] using radiochemical modeling techniques combined with recirculation line oxygen measurements, analyzed the responses of nine commercial BWRs to HWC. They showed that the abil-

ity of hydrogen added to the feedwater to reduce the oxygen in the recirculation system varied greatly from plant to plant.

Macdonald[2] and Macdonald et al.,[3] using Ruiz et al.'s calculated H_2, O_2, and H_2O_2 concentrations at various points around the primary HTC, estimated the ECP using a mixed potential model (MPM). They found that HWC, as described by Ruiz et al.,[1] was not effective in displacing the ECP of many in-vessel components to sufficiently negative values to achieve protection as the hydrogen added to the feedwater was increased. These components include the core and bypass structure, the upper plenum structures, and the downcomer. In some reactors, it was doubtful that HWC could protect the recirculation system and lower plenum, but in other reactors, these components were predicted to be protected by displacement of the ECP to values more negative than $-0.23 V_{SHE}$ (the value adopted by the U.S. Nuclear Regulatory Commission as the critical potential for IGSCC). Where comparisons could be made, the predictions of the MPM were in good agreement with the ECP data measured in operating BWRs, thereby lending credence to the viability of ECP modeling via the MPM.

Since these initial studies, we have developed a water radiolysis code (RADIOCHEM), which we have combined with the MPM and a crack growth rate (CGR) algorithm [the coupled environment fracture model[4–8] (CEFM)] to predict damage due to IGSCC and IASCC in BWR primary HTCs. The resultant code, DAMAGE-PREDICTOR, which is described in this paper (Part I of this series), is largely deterministic in nature in that the component models satisfy known physicochemical laws. The viability of this code is assessed by simulating the responses to HWC of the two reactors (Duane Arnold and Dresden-2) that were included in the original study of Ruiz et al.[1] We show that the predictions, which are described in Ref. 9 (Part II of this series), are in reasonable accord with those of Macdonald,[2] who used Ruiz et al.'s calculated values for $[H_2]$, $[O_2]$, and $[H_2O_2]$. Furthermore, we show (in the current paper) that the calculations are internally consistent in that a single set of parameters is able to describe the responses of these two quite different BWRs to HWC. In Ref. 10 (Part III of this series), we explore the responses of the two reactors to HWC under less than full-power conditions on the basis that HWC might be made effective in protecting in-vessel components if the plants are derated. Finally, in Ref. 11 (Part IV of this series), we discuss the new technique for enhancing the effectiveness of HWC by heterogeneous catalysis.

II. THEORETICAL BASIS

The structure of the DAMAGE-PREDICTOR algorithm used in this analysis is illustrated in Fig. 1. The water radiolysis model (RADIOCHEM), which calculates the concentrations of radiolysis products from the decomposition of water due to neutron and gamma irradiation, forms the base of this algoithm. The RADIOCHEM code takes into account the chemical reactions coupled to fluid convection to calculate the concentrations of the species at points around the HTC. Once the species concentrations have been determined in the whole primary HTC, the ECP is calculated using the MPM, and the CGR of a reference crack is also estimated using the CEFM. Auxiliary input parameters, such as flow velocity, coolant temperature, steam quality, and neutron and gamma dose rates in the coolant can be obtained from running other available software packages (such as TRAC and DOT-III).

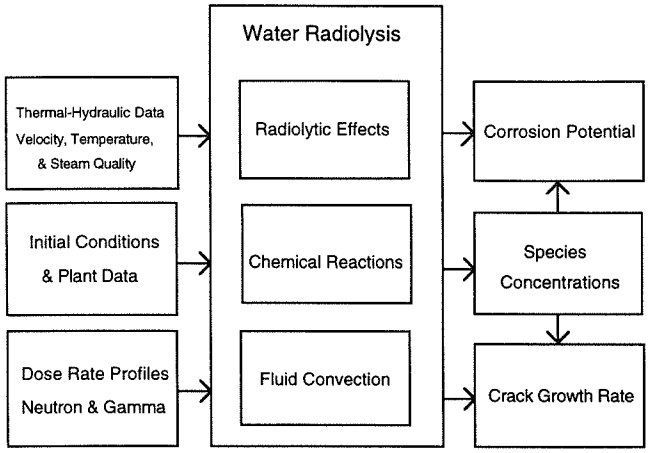

Fig. 1. Structure of the DAMAGE-PREDICTOR algorithm.

The nine regions of a BWR HTC that are specifically covered in this study are illustrated schematically in Fig. 2. The concentration of each species is calculated assuming one-dimensional transport.

II.A. Water Radiolysis

The fact that ~200 parts per billion (ppb) of oxygen is usually found in the BWR recirculation systems under normal operating conditions can be accounted for by the radiolysis of water in the HTCs. However, to explore the effectiveness of HWC, all radiolytic species distributions must be calculated because species other than oxygen are electroactive and hence will have an impact on the ECP and on the CGR. To calculate the species concentrations, one must carefully take into account the combined effects of the radiolytic yield of each species due to radiation and the changes in concentration due to chemical reactions and fluid convection.

Because of interaction between water molecules and neutron and gamma radiation, various molecules, ions, and radicals are created in the medium. The numbers of species i formed on the absorption of 100 eV of energy from neutrons and gamma photons are accounted

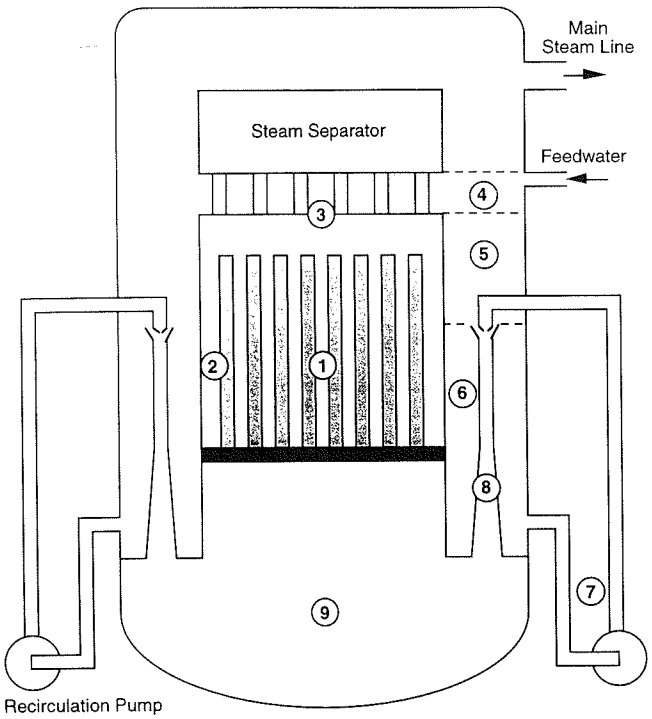

Fig. 2. Conceptual configuration of the BWR recirculation loop.

for by the parameters G_i^n and G_i^γ, respectively. Radiolytic yields (G values) for room temperature and high-temperature water are available from the research of Burns and Moore[12] and Lukashenko et al.[13] and are given in Table I.

Radiolysis is the primary source of most species in RADIOCHEM, and the rate at which any primary species is produced is given by

$$R_i^y = \left(\frac{G_i^\gamma \Gamma^\gamma}{100 N_v} + \frac{G_i^n \Gamma^n}{100 N_v} \right) \tilde{F} \rho \, dV \ , \qquad (1)$$

where

R_i^y is in units of mol/s

Γ^n = neutron dose rate (rad/s)

Γ^γ = gamma dose rate (rad/s)

N_v = Avogadro's number

$\tilde{F} = 6.25 \times 10^{13}$ (the conversion factor from rad/s to eV/g·s)

ρ = density of water (g/cm^3)

dV = liquid phase volume increment.

TABLE I

G Values for Primary Radiolytic Species in Water at 25 and 285°C

Number	Species	25°C		285°C	
		G^n	G^γ	G^n	G^γ
1	e^-	0.93	2.70	1.08	4.15
2	H	0.50	0.61	0.66	1.08
3	H^+	0.93	2.70	1.08	4.15
4	OH	1.09	2.86	0.26	3.97
5	OH^-	0.00	0.00	0.00	0.00
6	H_2O_2	0.99	0.61	0.74	1.25
7	HO_2	0.04	0.03	0.00	0.00
8	HO_2^-	0.00	0.00	0.00	0.00
9	O_2	0.00	0.00	0.00	0.00
10	O_2^-	0.00	0.00	0.00	0.00
11	H_2	0.88	0.43	0.00	0.62

The chemical reactions occurring in the HTCs of BWRs essentially determine the species concentrations in each part of the circuit, particularly in regions of low dose rate (i.e., in out-of-core regions). The reaction set used in this study is given in Table II, along with the rate constants and the activation energies. This reaction set is based on a published compilation[8] but has been modified to include hydrogen peroxide decomposition:

$$H_2O_2 \rightarrow H_2O + \tfrac{1}{2}O_2 \ . \qquad (2)$$

The rate of change of each species at a given location is given by elementary reaction rate theory as

$$R_i^c = \sum_{s=1}^{N} \sum_{m=1}^{N} k_{sm} C_s C_m \, dV - C_i \sum_{s=1}^{N} k_{si} C_s \, dV \ , \qquad (3)$$

where

k_{sm} = rate constant for the reaction between species s and m, which are the "parent" species, in the formation of species i

k_{si} = rate constant for the reaction between species s and i in the destruction of i

C_i = concentration of species i

C_m = concentration of species m

C_s = concentration of species s.

The rate constant k_j (j denotes the reaction number in Table II) is a function of coolant temperature. Because the temperature throughout the HTC is not constant, the actual rate constant for each chemical

TABLE II

Chemical Reaction Set Employed in RADIOCHEM

Number	Chemical Reactions	Rate Constant (25°C) (ℓ/mol·s)	Activation Energy (kcal/mol)
1	$e^- + H_2O = H + OH^-$	1.6×10^0	3.0
2	$e^- + H^+ = H$	2.4×10^{10}	3.0
3	$e^- + OH = OH^-$	2.4×10^{10}	3.0
4	$e^- + H_2O_2 = OH + OH^-$	1.3×10^{10}	3.0
5	$H + H = H_2$	1.0×10^{10}	3.0
6	$e^- + HO_2 = HO_2^-$	2.0×10^{10}	3.0
7	$e^- + O_2 = O_2^-$	1.9×10^{10}	3.0
8	$2e^- + 2H_2O = 2OH^- + H_2$	5.0×10^9	3.0
9	$2OH + H_2O = H_2O_2$	4.5×10^9	3.0
10	$OH + HO_2 = H_2O + O_2$	1.2×10^{10}	3.0
11	$OH + O_2^- = OH^- + O_2$	1.2×10^{10}	3.0
12	$OH^- + H = e^- + H_2O$	2.0×10^7	4.5
13	$e^- + H + H_2O = OH^- + H_2$	4.5×10^8	3.0
14	$e^- + HO_2^- + H_2O = OH + 2OH^-$	6.3×10^7	3.0
15	$H^+ + OH^- = H_2O$	1.44×10^{11}	3.0
16	$H_2O = H^+ + OH^-$	2.6×10^{-5}	3.0
17	$H + OH = H_2O$	2.0×10^{10}	3.0
18	$OH + H_2 = H + H_2O$	3.4×10^7	4.6
19	$OH + H_2O_2 = H_2O + HO_2$	2.7×10^7	3.45
20	$H + H_2O_2 = OH + H_2O$	4.4×10^7	4.5
21	$H + O_2 = HO_2$	1.9×10^{10}	3.0
22	$HO_2 = O_2^- + H^+$	8.0×10^5	3.0
23	$O_2^- + H^+ = HO_2$	5.0×10^{10}	3.0
24	$2HO_2 = H_2O_2 + O_2$	2.7×10^6	4.5
25	$2O_2^- + 2H_2O = H_2O_2 + O_2 + 2OH^-$	1.7×10^7	4.5
26	$H + HO_2 = H_2O_2$	2.0×10^{10}	3.0
27	$H + O_2^- = HO_2^-$	2.0×10^{10}	3.0
28	$e^- + O_2^- = HO_2^- + OH^-$	1.3×10^8	4.5
29	$OH^- + H_2O_2 = HO_2^- + H_2O$	1.8×10^8	4.5
30	$H_2O_2 = H_2O + \frac{1}{2}O_2$	0.2 (288°C)	
31	$H + H_2O = H_2 + OH$	1.04×10^{-4}	3.0
32	$H_2O + HO_2^- = H_2O_2 + OH^-$	1.02×10^4	3.0
33	$HO_2 + O_2^- = O_2 + HO_2^-$	1.5×10^7	4.5
34	$H_2O_2 = 2OH$	7.7×10^{-4}	7.3

reaction must be calculated for each specific position using Arrhenius' law:

$$k = k_0 \exp\left[\frac{E_a}{R}\left(\frac{1}{T_0} - \frac{1}{T}\right)\right], \qquad (4)$$

where

k_0 = rate constant at temperature T_0

E_a = activation energy

R = universal gas constant

T = temperature (K).

The rate constant for hydrogen peroxide decomposition (reaction 30) was calculated separately using an experimentally derived relationship[14]:

$$k_{30} = 1.4096 \times 10^5 \cdot \exp\left[-\left(\frac{14\,800}{RT}\right)\right]. \qquad (5)$$

As in all radiolysis models, we consider convection as the only mode of transport (i.e., we neglect diffusion and electromigration), and we assume that two-phase (water/steam) flow exists only in the reactor core. Single-phase (water) flow is assumed to exist in the other regions of the circuit, such as the core bypass and

the upper plenum. Thus, the rate of change of the number of moles of each species in volume element dV due to convection is

$$R_i^v = \frac{d(uC_i)}{dx}\, dV \ , \tag{6}$$

where u is the coolant velocity in the volume increment dV.

When coolant enters the bottom of the reactor core, the temperature of the coolant starts to increase because of the heat transfer from the fuel rods and by the deposition of energy directly in the water by neutrons and gamma photons. After the saturation temperature is reached, steam is produced, and the volume of the vapor phase expands from the point where boiling starts to the exit of the reactor core. When the vapor phase is formed, in addition to the formation of steam, mass transfer of dissolved gases occurs from the liquid phase to the vapor phase. A simplified model for describing mass transfer in two-phase flow was developed by Ibe et al.[15] The general expressions from that model for this process are given by

$$R_i^m = (\mu_i^* C_i^g - \mu_i C_i^f)\, dV_g$$

and

$$R_i^{m^*} = (\mu_i C_i^f - \mu_i^* C_i^g)\, dV_g \ , \tag{7}$$

where

f = liquid phase

g = vapor phase

dV_g = vapor phase volume increment

R_i^m = rate of change of species mole number in the liquid phase

$R_i^{m^*}$ = corresponding quantity in the vapor phase

μ_i^*, μ_i = gas release coefficient and gas absorption coefficient of species i, respectively, for mass transfer between the vapor phase and the liquid phase.

For want of a more comprehensive model for describing gas transfer in two-phase flow, this simplified model is used in RADIOCHEM.

II.B. General Solution

For a steady-state system, the total rate of change in the concentration of each species at each location is zero. Thus,

$$\left(\frac{G_i^\gamma \Gamma^\gamma}{100N_v} + \frac{G_i^n \Gamma^n}{100N_v}\right)\tilde{F}\rho\, dV + \left(\sum_{s=1}^{N}\sum_{m=1}^{N} k_{sm} C_s C_m - C_i \sum_{s=1}^{N} k_{si} C_s\right) dV + \left[\frac{d(uC_i)}{dx}\, dV\right] \pm (\mu_i^* C_i^g - \mu_i C_i^f)\, dV_g = 0 \ . \tag{8}$$

Because a one-dimensional calculation only is considered in the analysis, dV can be expressed as $A(x)dx$, where $A(x)$ is the cross-sectional area at a specific point x. Equation (8) can then be rewritten by replacing dV with $[A_f(x) + A_g(x)]\, dx$, where A_f and A_g are the cross-sectional areas of liquid and vapor, respectively. Accordingly,

$$\left(\frac{G_i^\gamma T^\gamma}{100N_v} + \frac{G_i^n \Gamma^n}{100N_v}\right)\tilde{F}\rho_f A_f(x)\, dx + \left(\sum_{s=1}^{N}\sum_{m=1}^{N} k_{sm} C_s^f C_m - C_i^f \sum_{s=1}^{N} k_{si} C_s^f\right) A_f(x)\, dx + [u_f(x) C_i^f(x) A_f(x) - u_f(x+dx) C_i^f(x+dx) A_f(x+dx)] + (\mu_i^* C_i^g - \mu_i C_i^f) A_g(x)\, dx = 0 \tag{9}$$

for the liquid phase and

$$\left(\frac{G_i^\gamma \Gamma^\gamma}{100N_v} + \frac{G_i^n \Gamma^n}{100N_v}\right)\tilde{F}\rho_g A_g(x)\, dx + \left(\sum_{s=1}^{N}\sum_{m=1}^{N} k_{sm} C_s^g C_m^g - C_i^g \sum_{s=1}^{N} k_{si} C_s^g\right) A_g(x)\, dx + [u_g(x) C_i^g(x) A_g(x) - u_g(x+dx) C_i^g(x+dx) A_g(x+dx)] + (\mu_i C_i^f - \mu_i^* C_i^g) A_g(x)\, dx = 0 \tag{10}$$

applies to the vapor phase, where

ρ_f = density of liquid water (g/cm^3)

ρ_g = density of steam (g/cm^3)

u_f = flow velocity in the liquid phase

u_g = flow velocity in the vapor phase.

Equation (10) can be further simplified by omitting the first two terms for the following reasons. First, the value derived from the first term is relatively small when compared with the values of the other terms mainly because the density of steam is small. Second, with the assumption that the steam is dry, there are only three species, $H_2O(g)$, H_2, and O_2, in the vapor phase. Because no highly reactive radical species are present, little chemical reaction is expected over the time of residence of steam in the vessel.

On linearizing the term $u(x+dx)C_i(x+dx) \times A(x+dx)$ by Taylor expansion and by neglecting the high-order terms, we find that

$$u(x+dx)C_i(x+dx)A(x+dx) \cong u(x)C_i(x)A(x) + u(x)C_i(x)\frac{\partial A(x)}{\partial x}\, dx + u(x)\frac{\partial C_i(x)}{\partial x} A(x)\, dx + \frac{\partial u(x)}{\partial x} C_i(x)A(x)\, dx \ . \tag{11}$$

Substituting Eq. (11) into Eq. (9) and rearranging terms yields

$$\frac{dC_i^f}{dx} = \frac{\tilde{F}\rho_f}{u_f}\left(\frac{G_i^\gamma \Gamma^\gamma}{100N_v} + \frac{G_i^n \Gamma^n}{100N_v}\right) + \frac{1}{u_f}\left(\sum_{s=1}^{N}\sum_{m=1}^{N} k_{sm} C_s^f C_m^f - C_i^f \sum_{s=1}^{N} k_{si} C_s^f\right) - C_i^f \frac{dA_f(x)}{A_f(x)dx} - \frac{C_i^f}{u_f}\frac{du_f}{dx} + \frac{1}{u_f}\frac{A_g(x)}{A_f(x)}(\mu_i^* C_i^g - \mu_i C_i^f) \ . \quad (12)$$

Similarly, substituting Eq. (11) into Eq. (10) gives

$$\frac{dC_i^g}{dx} = -C_i^g \frac{dA_g(x)}{A_g(x)dx} - \frac{C_i^g}{u_g}\frac{du_g}{dx} - \frac{1}{u_g}(\mu_i^* C_i^g - \mu_i C_i^f) \ . \quad (13)$$

In the core boiling region, the cross-sectional area of the vapor phase can be calculated by multiplying the total cross-section area A_0 by the void fraction α, as shown in Eq. (14):

$$A_g(x) = \alpha(x) A_0 \ . \quad (14)$$

Given Eq. (14), one can also derive the following equations:

$$A_f(x) = [1 - \alpha(x)] A_0 \ , \quad (15)$$

$$\frac{A_g(x)}{A_f(x)} = \frac{\alpha(x)}{1 - \alpha(x)} \ , \quad (16)$$

and

$$\frac{dA_f(x)}{A_f(x)} = \frac{A_0 d[1 - \alpha(x)]}{A_0[1 - \alpha(x)]} = -\frac{d\alpha(x)}{[1 - \alpha(x)]} \ . \quad (17)$$

Replacing the A_g and A_f terms in Eq. (12) with the void fraction, we obtain

$$\frac{dC_i^f}{dx} = \frac{\tilde{F}\rho_f}{u_f}\left(\frac{G_i^\gamma \Gamma^\gamma}{100N_v} + \frac{G_i^n \Gamma^n}{100N_v}\right) + \frac{1}{u_f}\left(\sum_{s=1}^{N}\sum_{m=1}^{N} k_{sm} C_s^f C_m^f - C_i^f \sum_{s=1}^{N} k_{si} C_s^f\right) + C_i^f \frac{d\alpha(x)}{[1 - \alpha(x)]\,dx} - \frac{C_i^f}{u_f}\frac{du_f}{dx} + \frac{1}{u_f}\frac{\alpha(x)}{1 - \alpha(x)}(\mu_i^* C_i^g - \mu_i C_i^f) \ . \quad (18)$$

Similarly, for the concentration change in the vapor phase, the following equation is derived:

$$\frac{dC_i^g}{dx} = -C_i^g \frac{d\alpha(x)}{\alpha(x)\,dx} - \frac{C_i^g}{u_g}\frac{du_g}{dx} - \frac{1}{u_g}(\mu_i^* C_i^g - \mu_i C_i^f) \ . \quad (19)$$

By solving Eqs. (18) and (19) numerically, we are able to calculate the concentrations of each species at any point in a BWR HTC. In the actual numerical simulation, all the parameters except the flow velocity and the void fraction in Eqs. (18) and (19) were obtained from the published literature.[12-17] Rate constants for the chemical reactions and the radiolytic yields for the primary species have already been given, although the rate constant of the decomposition of H_2O_2 and the gas release and absorption coefficients were employed as adjustable parameters when calibrating RADIOCHEM against an operating reactor (Dresden-2). The gas release and absorption coefficients that were determined by this procedure are shown in Table III. A detailed discussion of the flow velocity and void fraction derivation is presented in Sec. II.C.

II.C. Heat Transfer in the Primary Circuits of Boiling Water Reactors

To solve Eqs. (18) and (19) for the concentration of each species in a BWR HTC, one needs a heat transfer model for calculating the void fraction distribution in the core region and the temperature and the flow velocity at any desired point of the circuit.[18,19] At this stage of development of DAMAGE-PREDICTOR, a simplified thermal-hydraulic code, named ZEBRA, is used for the reactor core thermal-hydraulic analysis. The ZEBRA code was developed by Blakeslee[18] and is somewhat easier to apply than the more comprehensive codes, such as the transient reactor analysis code[19] (TRAC-BD1/MOD1). The ZEBRA code calculates the temperatures of fuel, cladding, and coolant in the reactor core if specific plant data are supplied. Furthermore, the heat transfer coefficient and steam quality versus core height are also obtained. The shortcoming of ZEBRA is that subcooled boiling is not taken into account, although homogeneous, two-phase flow is assumed in the algorithm. However, at the current stage of development of DAMAGE-PREDICTOR, ZEBRA

TABLE III

Gas Release and Absorption Coefficients for Hydrogen and Oxygen

Coefficient	O_2	H_2
Gas release μ (s^{-1})	228	255
Gas absorption μ^* (s^{-1})	21.5	15.0

is still useful for performing the thermal-hydraulic analysis in the BWR core. Although the flow velocity and void fraction are not provided in the output of ZEBRA, they can be calculated using Bankoff's equation and mass balance.

According to Bankoff's equation[20] for bubbly flow, the void fraction and slip ratio (S) can be expressed as

$$\alpha = \frac{K}{1 - \left(\frac{1-q}{q}\right)\frac{\rho_g}{\rho_f}}$$

and

$$S = \frac{V_g}{V_f} = \frac{1-\alpha}{K-\alpha} \ , \qquad (20)$$

where

$K = 0.71 + 0.0001P$

P = system pressure (psia)

q = steam quality

V_g = steam flow velocity (cm/s)

V_f = liquid flow velocity (cm/s).

Also, from mass balance, we obtain

$$\rho_g V_g \alpha + \rho_f V_f (1-\alpha) = \rho_f V_{in} \ , \qquad (21)$$

where V_{in} is the liquid velocity at the core channel inlet. Combining Eqs. (20) and (21), we obtain

$$V_f = \frac{\rho_f V_{in}}{\alpha \rho_g S + (1-\alpha)\rho_f} \qquad (22)$$

and

$$V_g = S V_f \ . \qquad (23)$$

Equations (20) through (23) are required for evaluating the species concentrations in the BWR core region in the presence of two-phase flow. For the other regions, with single-phase flow, constant velocity and linear temperature distributions are assumed.

II.D. Neutron and Gamma Dose Rate Profiles

The importance of accurately simulating the neutron and gamma dose rates in the primary circuit, especially in the downcomer region, has been previously emphasized.[1,15] The radiolytic decomposition of water and the decomposition of hydrogen peroxide in the downcomer region are believed to be important factors in determining the oxygen concentration in the recirculation line. The dose rate profiles must be supplied for the primary HTC of the plant to be analyzed, although neutron transport codes, such as DOT-III, have been developed in the past for calculating the dose rate profiles. In the current study, the dose rate data were obtained from Ref. 1.

II.E. Numerical Simulation

Equations (18) and (19) were solved for closely spaced locations around the coolant circuit (Fig. 3) using an implicit iterative procedure that employed Newton's method with a trapezoidal rule.[21] This method is fast (~22 min for four iterations on a DEC-3000 work station or ~3 h on a Pentium personal computer) and has acceptable accuracy. A total of nine nodes with an initial step size of 1×10^{-12} cm and a normal step size of 0.2 cm were employed in the integration, thereby yielding effectively continuous distributions in the calculated properties around the coolant circuit. Full details of the integration procedure are given in Ref. 22.

The initial conditions applied to any case study for estimating species concentrations are generally the same, except that the concentration of oxygen may be different from case to case. The concentrations of species other than H^+, OH^-, and O_2 are assumed to be zero. The concentrations of H^+ and OH^- are calculated from the dissociation product of water using the following equations[23]:

$$pK_w = \frac{4466.2}{T} - 5.941 + 0.016638T \ , \qquad (24)$$

$$C_{H^+} = 10^{-(pK_w/2)} \ , \qquad (25)$$

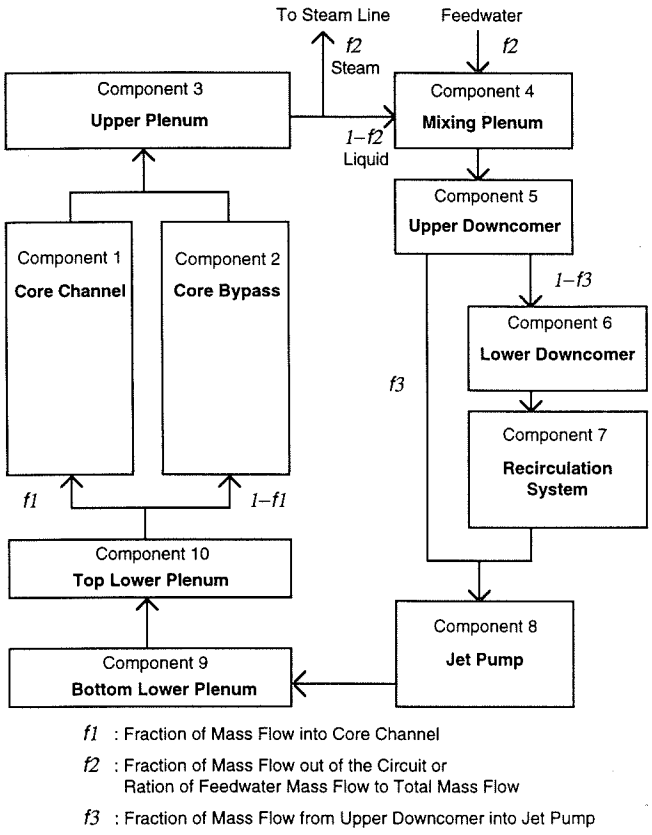

Fig. 3. Conceptual flow pattern in BWR HTC.

and

$$C_{OH^-} = \frac{K_w}{C_{H^+}} , \quad (26)$$

where T is the temperature in kelvin. The initial concentration of O_2 is taken from plant data for normal water chemistry conditions. For example, an initial concentration for O_2 of 200 ppb was used in our previous study[22] of the Dresden-2 BWR. This initial concentration was measured in the recirculation system.

II.F. Mixed Potential Model

After the concentration of each radical species is calculated, the corrosion potential of the component can be calculated using the MPM (Refs. 2 and 3), which is based on the physical condition that charge conservation must be obeyed at the steel surface. Because electrochemical reactions transfer charge across a metal-solution interface at rates measured by the partial currents, Eq. (27) expresses the charge conservation constraint for a uniformly accessible surface as follows:

$$\sum_{j=1}^{n} i_{R/O,j}(E) + i_{corr}(E) = 0 , \quad (27)$$

where $i_{R/O,j}$ is the partial current density due to the j'th redox couple in the system and i_{corr} is the corrosion current density of the material. These partial currents depend on the potential drop across the metal-solution interface.

The current density $i_{R/O}$ for a redox couple

$$R \Leftrightarrow O + ne \quad (28)$$

(where R is the reduced species and O is the oxidized species) can be expressed in terms of a generalized Butler-Volmer equation as

$$i_{R/O} = \frac{\exp[(E - E^e_{R/O})/b_a] - \exp[-(E - E^e_{R/O})/b_c]}{\frac{1}{i_{0,R/O}} + \frac{1}{i_{l,f}} \exp[(E - E^e_{R/O})/b_a] - \frac{1}{i_{l,r}} \exp[-(E - E^e_{R/O})/b_c]} , \quad (29)$$

where

$i_{0,R/O}$ = exchange current density

$i_{l,f}$ = mass-transfer-limited current for the forward direction of the redox reaction

$i_{l,r}$ = mass-transfer-limited current for the reverse direction of the redox reaction

b_a = anodic Tafel constant

b_c = cathodic Tafel constant

$E^e_{R/O}$ = equilibrium potential for this reaction as computed from the Nernst equation:

$$E^e_{O/R} = E^0_{O/R} - \frac{2.303RT}{nF} \log\left(\frac{a_R}{a_O}\right) , \quad (30)$$

where

a_R = thermodynamic activity of R

a_O = thermodynamic activity of O

$E^0_{O/R}$ = standard potential.

Limiting currents are calculated using the equation

$$i_{l,O/R} = \pm 0.0165 nFDC^b_{O/R} \mathrm{Re}^{0.86} \mathrm{Sc}^{0.33}/d , \quad (31)$$

where

F = Faraday's number

D = diffusivity of the redox species

$C^b_{O/R}$ = bulk concentration of O or R, as appropriate

Re = Reynolds number (Re = Vd/ν)

Sc = Schmidt number (Sc = ν/D)

d = channel diameter

V = flow velocity

ν = kinematic viscosity

and the sign depends on whether the reaction is in the forward (+) or reverse (−) direction.

The redox reactions of interest in this study are

$$H_2 \Leftrightarrow 2H^+ + 2e^- ,$$
$$O_2 + 4H^+ + 4e^- \Leftrightarrow 2H_2O ,$$
$$H_2O_2 + 2H^+ + 2e^- \Leftrightarrow 2H_2O . \quad (32)$$

Using the data available from the published literature for the various constants and the coefficients,[2–4,24,25] one can calculate the ECP using Eq. (29).

II.G. Coupled Environment Fracture Model

After the concentration of each electroactive species and the corrosion potential are calculated, the CGR of any existing crack can be estimated using CEFM (Refs. 4 through 8).

The basic assumption of the CEFM is that crack advance occurs via the slip/dissolution/repassivation mechanism, but the governing physicochemical condition is the conservation of charge. In the case of a crack, this condition is expressed as

$$i_{crack} A_{crack} + \int_S i^N_c \, dS = 0 , \quad (33)$$

where

i_{crack} = current density existing at the crack mouth (which may be different from that at the crack tip if cathodic reactions occur within the crack)

A_{crack} = area of the crack mouth

i_c^N = net (cathodic) current density due to charge transfer reactions on the external surface

S = surface area of the material outside the crack

dS = increment of the surface area.

Figure 4 demonstrates the physicoelectrochemical basis of the CEFM. Accordingly, the net cathodic current density at any point on the external surface can then be expressed as

$$i_c^N = i(H_2) + i(O_2) + i(H_2O_2) + i_{diss} \ , \qquad (34)$$

where $i(H_2)$, $i(O_2)$, and $i(H_2O_2)$ are the partial current densities for the redox reactions and i_{diss} is the dissolution current density of the metal. For calculating the cathodic current density of species X, the Butler-Volmer equation, as shown in Eq. (29), can once again be used to yield

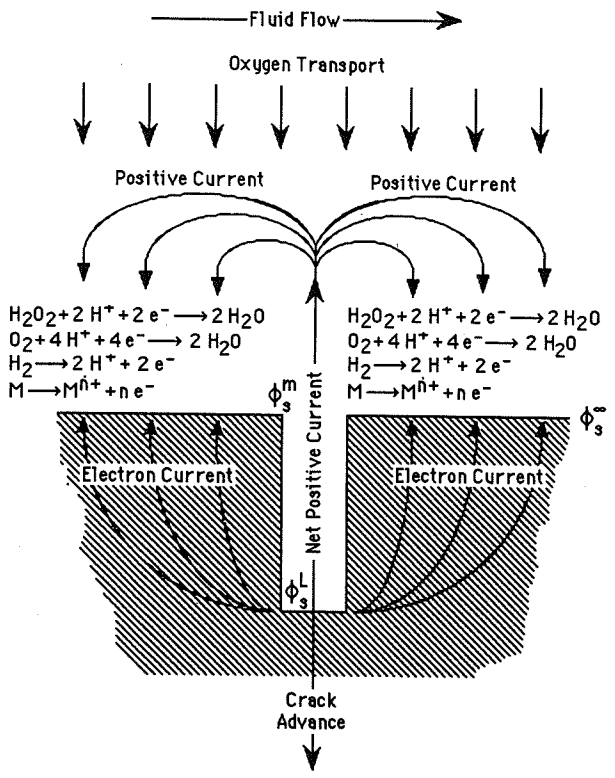

Fig. 4. Illustration of theoretical basis for CEFM.

$$i(X) = \frac{\exp[(\phi_s - \phi_s^e)/b_a] - \exp[-(\phi_s - \phi_s^e)/b_c]}{\frac{1}{i_0} + \frac{1}{i_{i,f}} \exp[(\phi_s - \phi_s^e)/b_a] - \frac{1}{i_{i,r}} \exp[-(\phi_s - \phi_s^e)/b_c]} \ , \qquad (35)$$

where ϕ_s is the electrostatic potential in the solution with respect to the metal adjacent to the surface, ϕ_s^e is the corresponding quantity at equilibrium, and the other parameters are as defined Sec. II.F. To find the potential distribution at the external surface, we must solve Laplace's equation

$$\nabla^2 \phi_s = 0 \qquad (36)$$

for the appropriate boundary conditions. Once the current density for each species is determined, the algorithm yields the total current I_{total} emanating from the crack mouth and hence the CGR.

In solving this problem, we note that the average current flowing out of the crack tip over a slip/dissolution/repassivation cycle can be calculated[4] by

$$\bar{I}_0 = 2 i_0^0 A_t^0 \left(\frac{t_0}{t_f}\right)^{1/2} \exp[-(\phi_s^L - \phi_s^0)/b_a] \ , \qquad (37)$$

where

i_0^0 = standard exchange current density for metal dissolution

A_t^0 = crack tip area

ϕ_s^L = potential in the solution adjacent to the crack tip (Fig. 4)

ϕ_s^0 = standard potential for the crack tip dissolution reaction on the solution side

t_f = time of cyclic fracture of the passive film at the crack tip

t_0 = constant determined from the repassivation transient.

The potential ϕ_s^L has to be derived using iterative trial and error to meet the requirement of electrical neutrality inside the crack (this condition is applied at the crack tip) and to satisfy the requirement that $I_{total} = \bar{I}_0$. Finally, the CGR can then be determined from Faraday's law, which yields

$$\frac{dL}{dt} = \frac{M \bar{I}_0}{2 \rho_m z F A_t^0} \ , \qquad (38)$$

where

L = length of the crack

M = atomic weight of the metal

ρ_m = metal density

z = metal oxidation number.

The fracture frequency of the passive film at the crack tip is equal to the inverse of the fracture period:

$$f_r = \frac{1}{t_f} = \frac{\dot{\epsilon}}{\epsilon_f} , \tag{39}$$

where $\dot{\epsilon}$ is the strain rate in inverse seconds and ϵ_f is the strain of the passive film at the crack tip at fracture. According to Ford et al.,[26] the crack tip strain rate is related to the stress intensity factor by an empirical relation, $\dot{\epsilon} = 4.11 \times 10^{-14} K_I^4$, from which we derive the fracture frequency ($f_r = \dot{\epsilon}/\epsilon$) for an assumed strain at fracture of the passive film at the crack tip of $\epsilon = 0.001$. Thus,

$$f_r = 4.11 \times 10^{-11} K_I^4 \ (\mathrm{s}^{-1}) , \tag{40}$$

where K_I is the stress intensity factor in MPa·$\sqrt{\mathrm{m}}$. However, one must note that Eq. (40) is purely empirical. For this reason, we have sought a more mechanistically based method for calculating the crack tip strain rate and hence the fracture frequency of the passive film at the crack tip. Thus, Congleton et al.[27] proposed an analytical approach for calculating the crack tip strain rate as

$$\dot{\epsilon} = \frac{\dot{\delta}}{x} = \frac{1}{x}\left[\frac{\alpha \dot{J}}{\sigma_y} + \beta\left(\frac{\sigma_y}{E}\right)\dot{a}\cdot\ln\left(\frac{R}{x}\right)\right] , \tag{41}$$

where

$\dot{\delta}$ = crack opening displacement rate

x = length parameter ranging from 0.1 to 0.01 mm

α, β = constants

σ_y = yield strength

E = Young's modulus

$\dot{a}$ = CGR (dL/dt).

The parameter R is defined as

$$R = \frac{0.2EJ}{\sigma_y^2} , \tag{42}$$

where

$J = (1 - \nu^2)K_I^2/E$

ν = Poison's ratio

K_I = stress intensity factor.

The other important parameter $\dot{J}$ is defined as

$$\dot{J} = 63.653\pi J\dot{a} . \tag{43}$$

Given a typical value for ϵ (e.g., 0.001), the fracture frequency can be calculated using Eq. (39).

The methodology of calculating the crack growth velocity is different when using Ford's expression for the crack tip strain rate and when using Congleton's expression. While it is straightforward to derive the CGR by substituting Eqs. (37), (39), and (40) into Eq. (38) (after solving for the current and potential distributions), Congleton's method imposes the additional difficulty that the CGR appears on the right sides of Eqs. (41) and (43). Thus, the problem must be solved iteratively until a certain tolerance is met.

Crack growth rates calculated using the CEFM and the two approaches for estimating the crack tip strain rate are plotted in Fig. 5 as a function of ECP and conductivity (0.1 and 0.5 μS/cm at ambient temperature). Because the crack tip parameters are poorly known, we have calibrated the CEFM against the single CGR/ECP datum shown in Fig. 5, assuming that the ambient temperature conductivity is 0.1 μS/cm (note that the conductivity at 288°C is much higher). In all subsequent calculations, no parameter values were changed. We have also plotted in Fig. 5 representative experimental CGR/ECP data taken from Ford et al.[26] as well as the Ford/Andresen[26] CGR/ECP correlations for ambient temperature conductivities of 0.1, 0.2, and 0.3 μS/cm. At very negative ECP values, the CGR becomes independent of ECP. In the CEFM, this limit is modeled[8] using the void nucleation creep model of Wilkinson

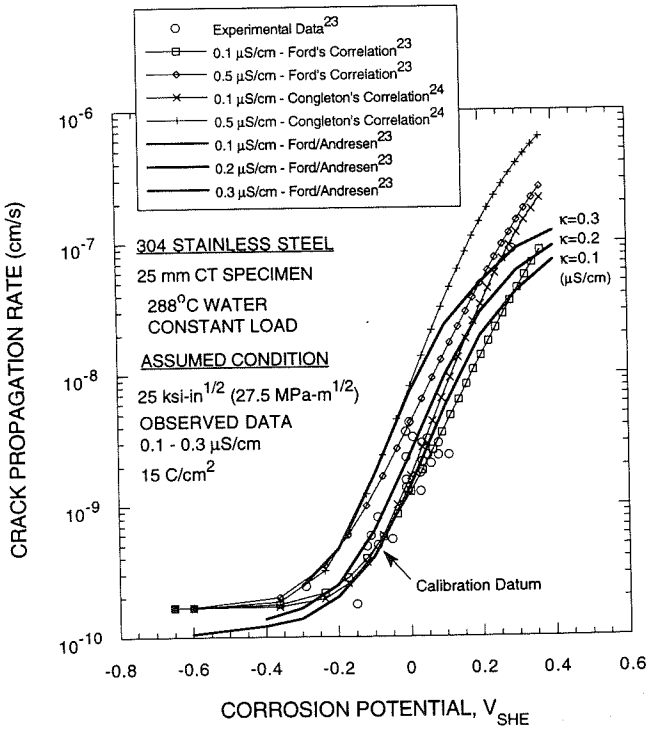

Fig. 5. Measured and calculated (using CEFM) CGR of sensitized Type 304 stainless steel as a function of corrosion potential.

and Vitek,[28] whereas in the Ford/Andresen model, the limit appears as a consequence of the function chosen to fit CGR versus ECP data. In any event, the CEFM, when calibrated against a single datum, provides an excellent account of the experimental data and is in good agreement with the correlations of Ford and Andresen,[26] provided that ECP $< 0.25 V_{SHE}$. However, the CEFM does predict a lower dependence of CGR on conductivity than indicated by the Ford/Andresen model. In this regard, we note that the Ford/Andresen correlation was apparently established using ambient temperature conductivity data, which are only marginally relevant in describing the transport properties of the environment at the elevated temperature. On the other hand, the CEFM uses the conductivity at the temperature of interest, as calculated from limiting ionic conductances, when solving for the current and potential distributions in the crack internal and external environments.

In the calculations reported here and in Refs. 9 and 10, we assume a "reference crack" of 0.5-cm length in a Type 304 stainless steel matrix, sensitized to an electrokinetic polarization reverse (EPR) value of 15 C/cm^2, and loaded mechanically to a stress intensity of 27.5 MPa$\cdot\sqrt{\text{m}}$. We recognize that a wide spectrum exists in crack length, sensitization (EPR value), and load in an actual reactor HTC, which is not represented by the calculations reported here. However, by maintaining the foregoing parameters constant, a clearer picture is obtained of the impact of the environment on crack growth, which is a primary goal of this work.

III. RESULTS AND DISCUSSION

The calibration of DAMAGE-PREDICTOR was done by matching the calculated oxygen concentrations in the recirculation system of Dresden-2 under HWC with the measured data, using the least-squares-fitting method.[22] To obtain the desired calculated oxygen concentration, we adjusted the gas transfer coefficients in the core boiling channels and the rate constant for the decomposition of hydrogen peroxide (reaction 30, Table II). We found that k_{30} had to be multiplied by a factor of 10 and the gas transfer coefficients had to take on the values summarized in Table III to achieve a good fit of RADIOCHEM to the Dresden-2 recirculation system oxygen data. The same set of gas transfer coefficients and the adjusted value for the rate constant (k_{30}) were then employed to simulate HWC in Duane Arnold.[22]

Comparison of the calculated and measured recirculation system oxygen levels for the two plants is given in Figs. 6 and 7. In general, this unique set of gas transfer coefficients (Table III) and the modified value for k_{30} yield an accurate simulation of the recirculation oxygen levels in these two plants that exist at opposite ends of the spectrum of plants explored by Ruiz et al.[1]

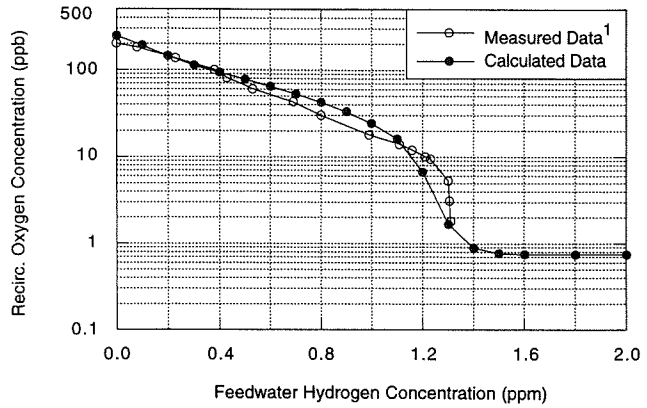

Fig. 6. Effect of hydrogen addition on the oxygen concentration in the recirculation line exit of Dresden-2.

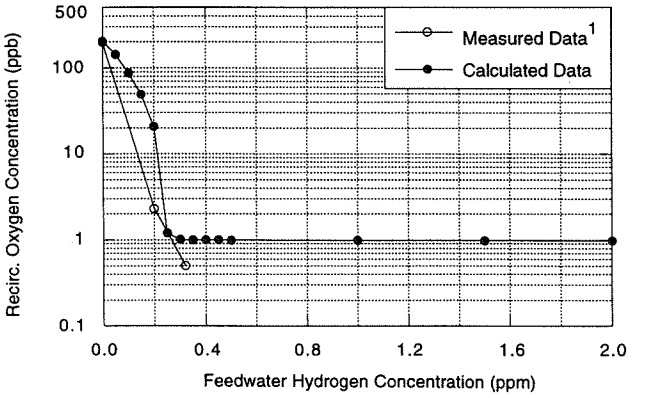

Fig. 7. Effect of hydrogen addition on the oxygen concentration in the recirculation line exit of Duane Arnold.

In addition to oxygen in the recirculation system, the calculated concentrations of oxygen and hydrogen in the main steam line are also compared with plant data in Figs. 8 through 11. The measured steam-line hydrogen concentration data were taken from the upper and the lower bound values of the nine plants reported in Ref. 1 because no hydrogen data for each individual plant are available. Again, we obtained excellent agreement, recognizing that the plant data are probably no more accurate than ±20% because of sampling errors.

The ECP data measured in a remote autoclave connected to the recirculation system of Duane Arnold[29] are compared with the calculated data in Fig. 12 for three flow velocities. The higher flow velocity (470 cm/s) corresponds to full-flow conditions in the recirculation piping system and hence cannot be taken as being representative of the autoclave sampling system. On the

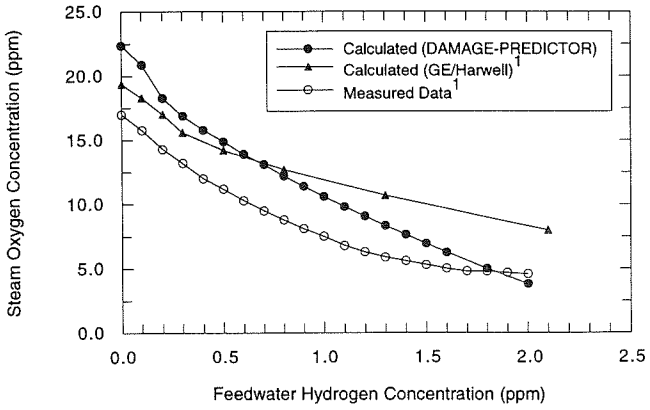

Fig. 8. Oxygen variations in the main steam line of Dresden-2 due to added hydrogen.

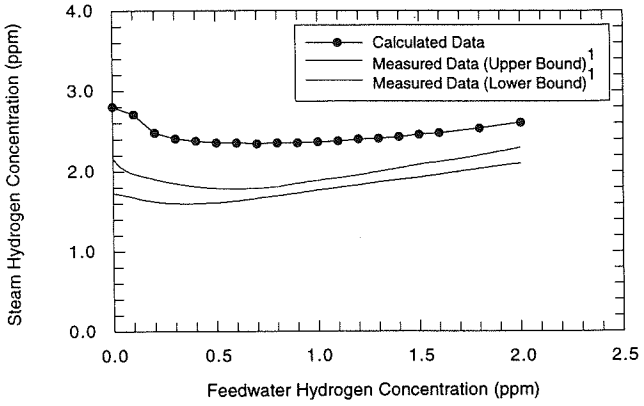

Fig. 10. Hydrogen variations in the main steam line of Dresden-2 due to added hydrogen.

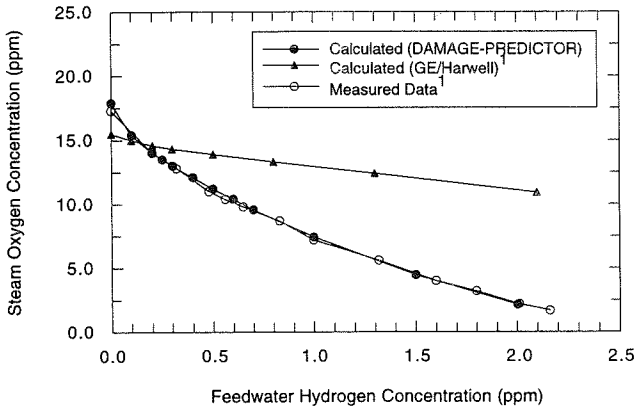

Fig. 9. Oxygen variations in the main steam line of Duane Arnold due to added hydrogen.

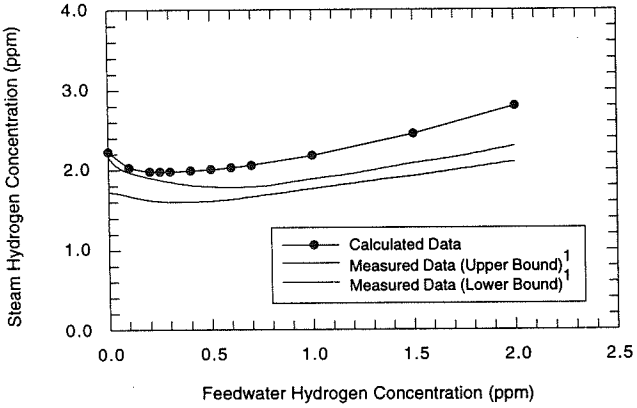

Fig. 11. Hydrogen variations in the main steam line of Duane Arnold due to added hydrogen.

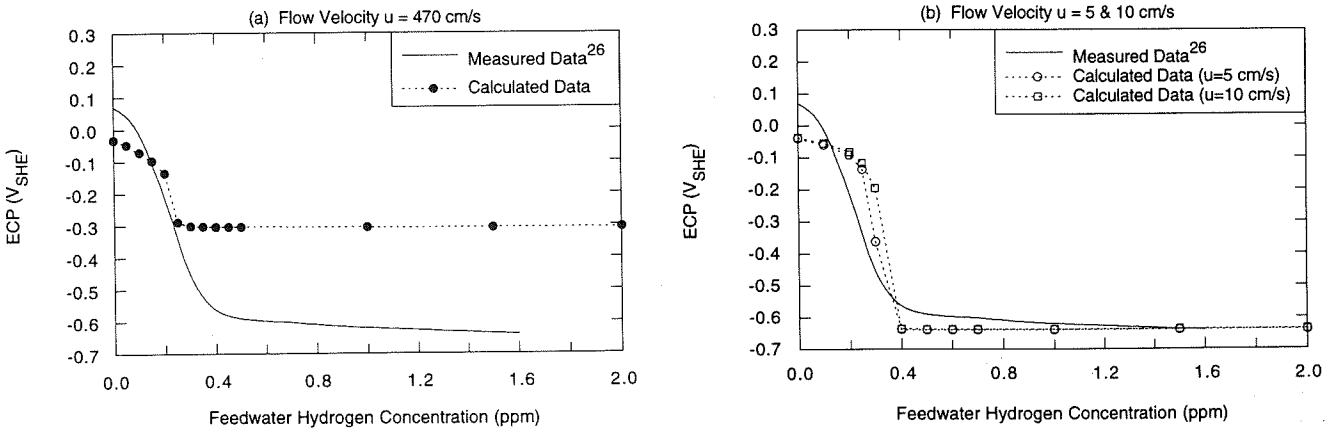

Fig. 12. Comparison of measured and calculated ECP variations at different flow velocities in the recirculation line of Duane Arnold under HWC.

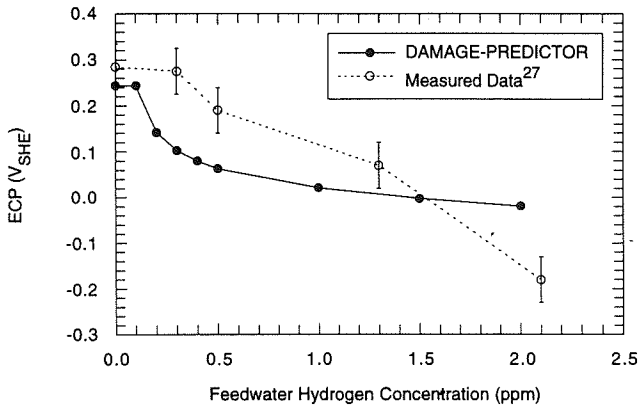

Fig. 13. Comparison of measured and calculated ECP variations at upper core bypass of Duane Arnold under HWC.

other hand, the lower flow velocities are representative of an autoclave, taking into account thermal convection. Accordingly, we regard the level of agreement between the calculated and the plant data to be excellent, given that the hydrodynamic conditions in the autoclave, in which the ECP measurements were made, are unknown. Furthermore, we expect that the oxygen and hydrogen peroxide concentrations might also have changed in the sampling line and these changes could affect the ECP. These findings illustrate the need to carefully design ECP monitoring systems so that the local hydrodynamic parameters (flow velocity and hydrodynamic diameter) are known.

The ECP measurements in the core bypass of Duane Arnold[29] are also compared with the calculated data in Fig. 13. For feedwater hydrogen concentration <1.5 parts per million (ppm), the ECP predicted by DAMAGE-PREDICTOR is ~100 mV lower than the measured data. However, we point out that the ECP-measuring electrode was placed inside the local power range monitor (LPRM) housing tube. Because the hydrodynamic diameter of the LPRM tube is different from that of the core bypass, the flow velocity in the LPRM tube will also be different. Therefore, based on the previous discussion, one would expect the measured ECP values to deviate from the calculated values for the bypass shown in Fig. 13. In addition, based on our extensive experience in high-temperature aqueous electrochemistry, we do not believe the measured ECP could be any more accurate than ±50 mV. We have indicated this level of uncertainty on the measured points plotted in Fig. 13.

Some modeling calculations, which relate to the oxygen and hydrogen peroxide concentrations and the CGR in the upper core bypass of Duane Arnold under HWC, were performed by Indig and Nelson,[30] who used the GE/Harwell model for estimating radiolysis species concentrations and the Ford-Andresen model for calculating CGRs. Their results are compared with the data predicted by DAMAGE-PREDICTOR in Figs. 14, 15, and 16. Because the chemical reaction set (Table II) employed by the GE/Harwell model is different from that used by DAMAGE-PREDICTOR, the calculated species concentrations from the two models are not expected to be in agreement. Furthermore, the CGRs calculated by the Ford-Andresen model were for a water conductivity of 0.15 μS/cm, which is higher than the 0.1 μS/cm considered in DAMAGE-PREDICTOR calculations. The difference in conductivity is a principal reason why the CGRs reported by Indig and Nelson[30] are higher than those predicted by DAMAGE-PREDICTOR. Thus, as estimated in Ref. 9, a doubling

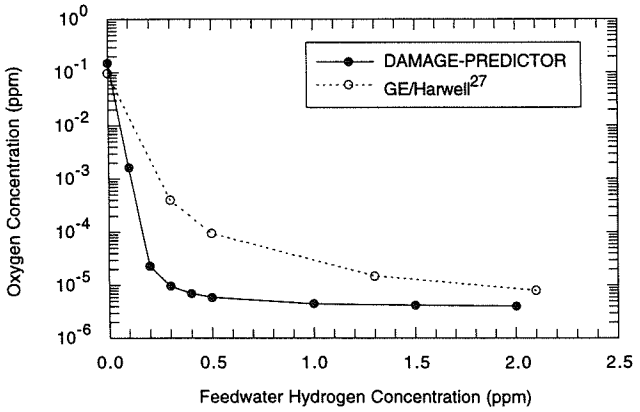

Fig. 14. Comparison of calculated oxygen concentrations by DAMAGE-PREDICTOR and the GE/Harwell model at upper core bypass of Duane Arnold under HWC.

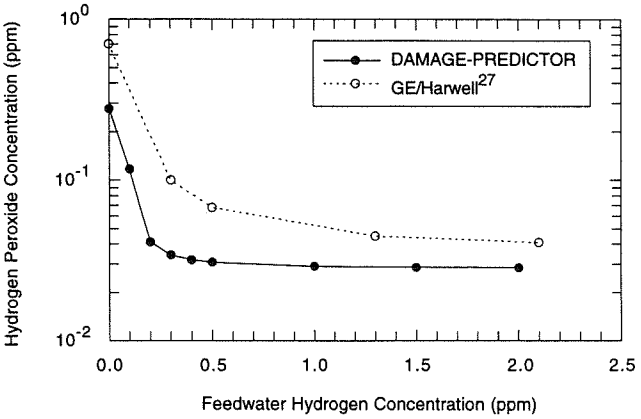

Fig. 15. Comparison of calculated hydrogen peroxide concentrations by DAMAGE-PREDICTOR and the GE/Harwell model at upper core bypass of Duane Arnold under HWC.

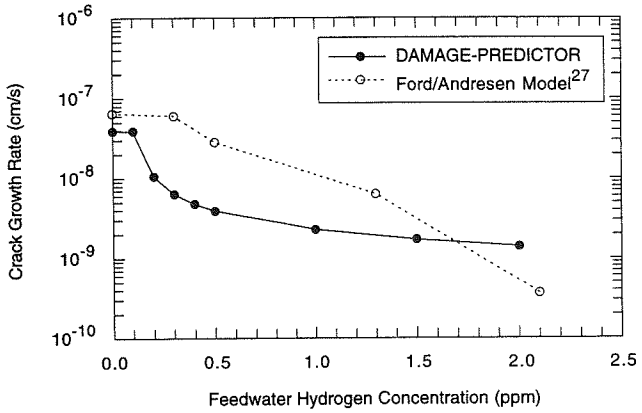

Fig. 16. Comparison of calculated CGRs by DAMAGE-PREDICTOR and by the Ford/Andresen model using measured ECP data for upper core bypass of Duane Arnold under HWC.

of the conductivity (0.1 to 0.2 μS/cm) at high ECP values results in an increase in the CGR by a factor of 2 to 6. The difference is predicted to be at the lower end of this range for lower ECP values, as the CGR approaches the creep limit. Accordingly, the difference in conductivity alone probably accounts for more than half of the difference in CGRs indicated in Fig. 16. The remaining difference is presumably due to the differences in the predicted concentrations of H_2, O_2, and H_2O_2, and to differences in the algorithms for estimating CGR.

IV. SUMMARY AND CONCLUSIONS

An algorithm (DAMAGE-PREDICTOR) was developed to model the water radiolysis, corrosion potential (ECP), and CGR behaviors of components in the primary coolant circuits of BWRs. The algorithm contains a deterministic model for calculating the concentrations of radiolysis products around the HTC, as a function of power level and the concentration of hydrogen in the reactor feedwater. The concentrations of hydrogen, oxygen, and hydrogen peroxide, together with thermal-hydraulic data, are used to calculate the corrosion potential via the deterministic MPM and the rate of growth of a reference crack (crack length = 0.5 cm, $K_I = 27.5$ MPa$\cdot\sqrt{\text{m}}$, and water conductivity at 25°C = 0.1 μS/cm) is calculated through the CEFM at any location within the HTC. The algorithm is initially calibrated against recirculation system oxygen levels for Dresden-2 by adjusting the rate constant for the decomposition of hydrogen peroxide and by modifying the gas release and absorption coefficients for oxygen and hydrogen within the boiling regions in the core. Without any further parameter changes, the algorithm successfully accounts for the recirculation system oxygen levels for Duane Arnold, for the steam-line O_2 and H_2 levels reported for Dresden-2 and Duane Arnold, and for ECP data measured in remote autoclaves connected to the recirculation system of Duane Arnold. Furthermore, the algorithm successfully accounts for in-core ECP data in Duane Arnold all as a function of hydrogen added to the reactor feedwater ($[H_2] = 0$ to 2 ppm). The fact that Dresden-2 and Duane Arnold display widely different responses to HWC, suggests that DAMAGE-PREDICTOR, once calibrated against one plant, may be applicable to a wide spectrum of BWRs.

REFERENCES

1. C. P. RUIZ et al., "Modeling Hydrogen Water Chemistry for BWR Applications," EPRI NP-6386, Electric Power Research Institute (June 1989).

2. D. D. MACDONALD, *Corrosion*, **48**, *3*, 194 (1992).

3. D. D. MACDONALD et al., "Estimation of Corrosion Potentials in the Heat Transport Circuits of LWRs," *Proc. Int. Conf. Chemistry in Water Reactors: Operating Experience & New Developments*, Nice, France, April 24–27, 1994, French Nuclear Energy Society.

4. D. D. MACDONALD and M. URQUIDI-MACDONALD, *Corros. Sci.*, **32**, 51 (1991).

5. D. D. MACDONALD and M. URQUIDI-MACDONALD, *Proc. 4th Int. Symp. Environmental Degradation of Materials in Nuclear Power Systems—Water Reactors*, Jekyll Island, Georgia, August 6–10, 1989, p. 4-1, National Association of Corrosion Engineers.

6. D. D. MACDONALD and M. URQUIDI-MACDONALD, *Proc. Parkins Symp. Fundamental Aspects of Stress Corrosion Crack*, Warrendale, Pennsylvania, 1992, p. 443, S. M. BRUEMMER, E. I. MELETIS, R. H. JONES, W. W. GERBERICH, F. P. FORD, and R. W. STAEHLE, Eds., The Metallurgical Society.

7. D. D. MACDONALD, M. URQUIDI-MACDONALD, and P. C. LU, "The Coupled Environment Fracture Model—A Deterministic Method for Calculating Crack Growth Rates," presented at CORROSION/94, Baltimore, Maryland, February 28–March 4, 1994, NACE International.

8. D. D. MACDONALD, P. C. LU, M. URQUIDI-MACDONALD, and T.-K. YEH, "Theoretical Estimation of Crack Growth Rates in Type 304 Stainless Steel in BWR Coolant Environments," *Corrosion* (submitted for publication) (1995).

9. T.-K. YEH and D. D. MACDONALD, "Modeling Water Chemistry, Electrochemical Corrosion Potential, and Crack Growth Rate in the Boiling Water Reactor Heat Transport Circuits—II: Simulation of Operating Reactors," *Nucl. Sci. Eng.* (submitted for publication).

10. T.-K. YEH and D. D. MACDONALD, "Modeling Water Chemistry, Electrochemical Corrosion Potential, and Crack Growth Rate in the Boiling Water Reactor Heat Transport Circuits—III: Effect of Reactor Power Level," *Nucl. Sci. Eng.* (submitted for publication).

11. T.-K. YEH and D. D. MACDONALD, *Nucl. Sci. Eng.* (to be submitted for publication).

12. W. G. BURNS and P. B. MOORE, *Radiat. Eff.*, **30**, 233 (1976).

13. M. L. LUKASHENKO et al., *At. Energ.*, **72**, *6*, 570 (1992).

14. C. C. LIN et al., *Int. J. Chem. Kinet.*, **23**, 971 (1991).

15. E. IBE et al., *J. Nucl. Sci. Technol.*, **23**, *1*, 11 (1986).

16. J. CHUN, "Modeling of BWR Water Chemistry," Master Thesis, Department of Nuclear Engineering, Massachusetts Institute of Technology (1990).

17. D. D. MACDONALD and M. URQUIDI-MACDONALD, *Corrosion*, **46**, *5*, 380 (1990).

18. J. A. BLAKESLEE, "ZEBRA—A Computer Code for the Steady-State Thermal Analysis of Light Water Cooled Nuclear Power Reactor," Master Paper, Department of Nuclear Engineering, The Pennsylvania State University (1974).

19. "TRAC-BD1/MOD1: An Advanced Best Estimate Computer Program for Boiling Water Reactor Transient Analysis," *TRAC-BD1/MOD1 User's Manuals*, Vol. 1 (June 1992).

20. J. H. RUST, *Nuclear Power Plant Engineering*, S. W. Holland Company, Atlanta, Georgia (1979).

21. C. W. GEAR, *Numerical Initial-Value Problems in Ordinary Differential Equations*, Prentice Hall, Englewood Cliffs, New Jersey (1971).

22. T.-K. YEH, "The Viability of Hydrogen Water Chemistry for Mitigating Stress Corrosion Cracking in Boiling Water Reactor Heat Transport Circuits," PhD Thesis, Department of Nuclear Engineering, The Pennsylvania State University (1994).

23. A. B. NAUMOV et al., "Handbook of Thermodynamics Data USGS TRANS.," USGS-WRD-74-001, U.S. Geological Survey (1974).

24. D. D. MACDONALD et al., *Corrosion*, **44**, 186 (1988).

25. J. B. LEE, "Electrochemical Approach to Corrosion Problems of Several Iron-Nickel-Chromium Alloys in High Temperature, High Pressure Water," PhD Thesis, The Ohio State University (1978).

26. P. FORD et al., "Corrosion-Assisted Cracking of Stainless and Low-Alloy Steels in LWR Environments," Final Report, EPRI NP-5064M, Electric Power Research Institute (Feb. 1987).

27. J. CONGLETON et al., *Corros. Sci.*, **25**, 633 (1985).

28. D. S. WILKINSON and V. VITEK, *Acta Metall.*, **30**, 1723 (1982).

29. M. E. INDIG, "Recent Advances in Measuring ECPs in BWR Systems," *Proc. 4th Int. Symp. Environmental Degradation of Materials in Nuclear Power Systems—Water Reactors*, Jekyll Island, Georgia, August 6–10, 1989, p. 4-411, National Association of Corrosion Engineers.

30. M. E. INDIG and J. L. NELSON, *Corrosion*, **47**, *3*, 202 (1991).